All-*trans* retinoic acid enhances the antitumor effects of fimaporfin-based photodynamic therapy

Judith Jing Wen Wong[1], Susanne Lorenz[2] and Pål Kristian Selbo[1,*]

[1]Department of Radiation Biology, Institute for Cancer Research, The Norwegian Radium Hospital, Oslo University Hospital, Norway; judwon@rr-research.no (J.J.W.W.); selbo@rr-research.no (P.K.S.)

[2]Genomics Core Facility, Department of Core Facilities, The Norwegian Radium Hospital, Oslo University Hospital, Oslo, Norway; susanne.lorenz@rr-research.no (S.L.)

*****Correspondence: Pål Kristian Selbo, selbo@rr-research.no; Tel.: +47-22781469

Abstract: The vitamin A metabolite all-*trans* retinoic acid (ATRA; tretinoin) has anticancer potential; however, lack of clinical success has prevented its approval for solid tumors. Herein, we propose combining low-dose ATRA preconditioning with fimaporfin-based photodynamic therapy (ATRA+PDT) for the treatment of solid cancers. Compared to monotherapies, ATRA+PDT induced synergistic cytotoxic responses including promotion of apoptosis in colon and breast carcinoma cell lines. In human HT-29 colon cancer cells, the effect of ATRA+PDT on gene expression was evaluated by RNA sequencing (RNA-seq). The unfolded protein response (UPR) and retinoic acid-mediated apoptosis signaling were predicted as strongly activated canonical pathways after ATRA+PDT compared to PDT. During the first 20 days post-ATRA+PDT, we obtained significant anti-tumor responses in HT-29 xenografts, including complete responses in 2/5 mice. In conclusion, ATRA+PDT represent a novel combination therapy for solid tumors that should be further tested in immunocompetent preclinical models.

Keywords: ATRA, photodynamic therapy, unfolded protein response, apoptosis, carcinoma

Abbreviations:

ALDH1A1: aldehyde dehydrogenase 1 family member A1

ALP: alkaline phosphatase

ATF3: activating transcription factor 3

ATRA: all-*trans* retinoic acid (tretinoin)

DEG: differentially expressed gene

EGR1: early growth response 1

GSEA: gene set enrichment analysis

HDAC9: histone deacetylase 9

IFN: interferon

IGFBP6: insulin-like growth factor-binding protein 6

IPA: Ingenuity pathway analysis

LCN2: lipocalin 2

LD_{50}: light-dose inducing 50% reduction of cell viability

LPS: lipopolysaccharide

PCI: photochemical internalisation

PDT: photodynamic therapy

RAR: retinoic acid receptor

REG4: regenerating islet-derived protein 4

RNA-seq: RNA sequencing

ROS: reactive oxygen species

UPR: unfolded protein response

TNF: tumor necrosis factor

TPCS2a: disulfonated tetraphenyl chlorin (fimaporfin)

TUNEL: Terminal deoxynucleotidyl transferase (TdT) dUTP nick-end labeling

Introduction

ATRA is derived from vitamin A and plays a crucial role in biological processes, including embryonic development, immune responses, and vision, through binding and activation of the nuclear retinoic acid receptors RARα, RARβ, and RARγ [1]. Transcriptional activation by RARs induce differentiation, cell cycle arrest, anti-proliferative, and apoptosis-inducing effects [2], which make retinoids attractive in cancer therapy. ATRA is successfully used in the differentiation and apoptosis induction therapy of acute promyelocytic leukemia [1, 3] and is currently being studied to prevent or treat carcinoma [4]. However, lack of effects in solid tumors has limited clinical translation of ATRA due to several factors: ATRA formulation and administration is challenging due to its low aqueous solubility. In addition, ATRA is oxidized when exposed to heat, UV light, or oxygen [4] and has a very short plasma half-life (~45 min) [5]. Moreover, RARβ expression is frequently lost in solid tumors, or the RAR promoter is epigenetically silenced, resulting in ATRA resistance [6, 7]. Thus, there is a high need for new ATRA drug delivery or combinatorial strategies to overcome resistance and improve the survival of patients with solid tumors.

PDT is used clinically for the treatment of different solid cancers and is based on three non-toxic components: photosensitizer, light, and oxygen. Upon light activation of the photosensitizer, energy is transferred to molecular oxygen, resulting in generation of cytotoxic reactive oxygen species (ROS), of which singlet oxygen is the most common [8]. The use of differentiation-promoting agents, e.g., preconditioning with vitamin D, to enhance PDT efficacy was first demonstrated by Ortel *et al.* to improve 5-aminolevulinic acid (ALA)-based PDT. However, ATRA was only shown to slightly enhance the photosensitizing compound PpIX production compared to ALA alone (non-significant) and no enhanced cytotoxic effects

was demonstrated [9]. Currently, there is a lack of mechanistic evidence showing that ATRA preconditioning improves PDT of cancer.

In this study, we aimed to investigate the potential anti-cancer effects of ATRA+PDT using fimaporfin ($TPCS_{2a}$), the core photosensitizer drug used for the drug delivery technology photochemical internalization (PCI)[10]. Fimaporfin has been tested clinically in combination with bleomycin [11] and vaccine peptide/protein-based antigens [12]. Recently, PCI in combination with gemcitabine was shown to be safe and effective in a Phase I study for the treatment of unresectable extrahepatic cholangiocarcinoma [13].

Here, we show for the first time that combining ATRA+PDT results in synergistic cytotoxic responses in ATRA resistant colon and breast carcinoma cell lines compared to ATRA or PDT monotherapy. Mechanistically, we demonstrate that ATRA+PDT results in cell cycle arrest, increased apoptotic cell death, and a substantial reduction in cancer cell proliferation. RNA-seq of the human colorectal adenocarcinoma cell line HT-29 identified 1129 differentially expressed genes (DEGs) after ATRA+PDT compared to PDT. Pathway analysis of the RNA-seq data confirmed apoptosis signaling and identified activation of the unfolded protein response (UPR). Quantitative RT-PCR and Western blotting revealed that ATRA+PDT strongly elevated the stress-induced activating transcription factor 3 (ATF3). *In vivo*, one single treatment with ATRA+PDT induced significant anti-tumor effects during the first 20 days compared to no treatment in HT-29 tumor-bearing athymic nude mice, and was the only group that achieved complete responses.

Results

ATRA+PDT enhances cytotoxic responses in breast and colon cancer cells

We evaluated the cytotoxic response of 0.01 to 100 µM ATRA monotherapy for 48 hours in SKBR3, HCT116, and HT-29 cells. For all cell lines, the viability was > 50% at ATRA concentrations < 50 µM (**Supplementary Fig. S1**). While the physiological concentration of ATRA is in the nanomolar range in human plasma [14], pharmacological doses of ATRA results in plasma concentrations in the micromolar range [15]. Thus, a therapeutic relevant concentration of 0.1 µM ATRA was selected for the subsequent experiments and combined with fimaporfin-PDT (ATRA+PDT). We examined the cytotoxic effects of ATRA+PDT in five different cancer cell lines; two human colon cancer cell lines: HCT116 (ATRA-resistant) and HT-29 (moderately ATRA-resistant) [16] and the MC-38 mouse colon cancer cell line. Two human breast cancer cell lines were also included: SKBR3 (ATRA-sensitive) [17] and MDA-MB-231 (ATRA-resistant) [18].

The cells were preconditioned with 0.1 µM ATRA and subjected to fimaporfin ($TPCS2_a$)-PDT. In contrast to HCT116, enhanced cytotoxicity was observed in SKBR3 and HT-29 cells (**Fig. 1a**) and in MC-38 and MDA-MB-231 (**Supplementary Fig. S2a**). The dual P13K and mTOR inhibitor NVP-BEZ235 augments ATRA efficacy in leukemic cells [19] and was therefore tested in combination with ATRA+PDT. However, no additional effect was found when combining 0.1 µM ATRA+PDT with NVP-BEZ235 at concentrations ranging from 5-100 nM in HT-29 and HCT116 (**data not shown**). Changing the treatment sequence where PDT was performed prior to ATRA incubation did not have any effect on the cell viability, indicating the importance of preconditioning **(Supplementary Fig. S2b)**.

To further evaluate whether the effect of ATRA+PDT was synergistic in HT-29 and SKBR3, the observed effect on cell viability was compared to the theoretical additive effect. A significant difference was found indicating synergy between ATRA and PDT (**Fig. 1b**) and

supported with synergy calculations **(Supplementary Results**). The clonogenic assay revealed that ATRA+PDT significantly induced a 4-fold and 6-fold reduction of the colony-forming ability of HT-29 following 90- and 120-seconds light exposure, respectively, whereas ATRA monotherapy failed to significantly affect survival (**Fig. 1c**). The impact of ATRA+PDT on proliferation was also evaluated (**Fig 1d**). Strikingly, ATRA+PDT blocked SKBR3 and HT-29 proliferation and attenuated proliferation of the ATRA-resistant HCT116 cells. ATRA monotherapy did not affect the proliferation of HT-29 and HCT116, in contrast to the SKBR3 cells, where the proliferation was slightly reduced.

Light exposure of ATRA alone is not cytotoxic, and *ex vivo* light exposure of ATRA and fimaporfin does not lead to cytotoxic photoproducts

ATRA is *per se* light-sensitive, and we, therefore, wanted to explore if blue light exposure of ATRA would cause cytotoxic effects. However, ATRA+light did not affect cell viability (**Supplementary Fig. S3a**). Furthermore, no cytotoxic photoproducts of ATRA+$TPCS_{2a}$ *ex vivo* were observed **(Supplementary Results and Supplementary Fig. S3b**).

ATRA+PDT induce cell cycle arrest and enhance apoptosis

The cell cycle was analyzed using flow cytometry at 24 and 72 hours after light exposure (**Fig. 2a**)**.** ATRA monotherapy did not induce any significant change in the cell cycle distribution. In the PDT- or ATRA+PDT-treated HCT116 cells, a slight non-significant increase in G1 was observed 24 hours post light-exposure. At 72 hours, a G2/M accumulation was observed in PDT- or ATRA+PDT-treated HCT116 cells compared to the NT and ATRA treatment (non-significant).

At 24 hours post-PDT or -ATRA+PDT, HT-29 cells significantly accumulated in G2/M, in line with previous PDT-based studies [20, 21]. Specifically, 36.9-43.7% of PDT- or ATRA+PDT-treated cells accumulated in G2/M compared to 12.6-12.9% in NT or ATRA-treated cells ($p \leq 0.001$-0.002). A non-significant increase in G2/M accumulation in both PDT- and ATRA+PDT-treated HT-29 cells was also observed at 72 hours post-treatment. No statistically significant differences were found when comparing PDT- and ATRA+PDT-treated samples for HT-29 and HCT116. For SKBR3 cells, a slight increase in G2/M accumulation was observed 24 hours after PDT, whereas a G2/M accumulation for ATRA+PDT-treated cells was observed after 72-hour (non-significant).

As the anti-proliferation effect of ATRA+PDT increased with time (**Fig. 1d**), we decided to assess the apoptotic response (TUNEL assay) at both 24 and 72 hours after a light-dose inducing ~ 50% reduction of cell viability (LD_{50}). The apoptotic fraction 24 hours post-light was low for both SKBR3 and HT-29. In contrast, an increased apoptotic fraction was found in ATRA+PDT- and PDT-treated HCT116 cells; however, not significantly different (**Fig. 2a**) At 72 hours post-ATRA+PDT, a significantly, 2-fold higher apoptotic response (~ 17%) was detected in HT-29 ($p \leq 0.01$) compared to PDT (~ 8.5%). A higher apoptotic response was also detected in HCT116 and SKBR3 post-ATRA+PDT, although not significant compared to PDT (**Fig. 2b**).

We, therefore, assessed cleaved caspase-3 in HT-29 after ATRA+PDT. In line with the TUNEL data, no cleaved caspase-3 was detected 24 hours after light exposure (**data not shown**). At 72 hours post-light, increased cleaved caspase-3 was observed in PDT- and ATRA+PDT-treated cells (**Fig. 2c**). A tendency (non-significant) of higher expression of cleaved caspase-3 was observed after ATRA+PDT compared to PDT across all three

independent experiments. Altogether this indicates that increased cell death after ATRA+PDT is partly due to an enhanced apoptotic response.

Low-dose ATRA neither elevate intracellular ROS levels nor alkaline phosphatase (ALP) activity and CD133 expression

ATRA induces ROS generation in leukemia [22]. The intracellular ROS was therefore measured post-ATRA+PDT. As expected, an increase in DCF fluorescence, indicating enhanced ROS generation, was observed in all PDT-treated samples (**Fig. 2d**). Compared to PDT, ROS levels post ATRA+PDT showed a tendency to increase (~ 20%, non-significant) only in the SKBR3 cells. However, low-dose ATRA (0.1 µM) did not influence the ROS generation in all cell lines tested.

ALP is a marker of intestinal cell differentiation [23] and was used to evaluate treatment-induced differentiation. Cells were short-term incubated with ATRA concentrations up to 1 µM for 42 hours, harvested, and assayed. The basal ALP activity was high in SKBR3 and low in HCT116 and HT-29 (**Supplementary Fig. S4a**). ATRA did not significantly affect the ALP activity. Intriguingly, we observed a tendency of reduced (non-significant) ALP activity in ATRA-treated SKBR3 cells (**Supplementary Fig. S4a**).

The surface expression of the cancer stem cell marker CD133 was also evaluated using flow cytometry. The CD133 expression was slightly reduced (non-significant) in HT-29 cells after 42 hours incubation of 0.1-1 µM ATRA (**Supplementary Fig. S4b**). Altogether, short-term and low-dose ATRA treatment does not induce differentiation.

Differentially expressed genes (DEGs) after ATRA+PDT compared to PDT

As ATRA monotherapy did not have any effect on cell viability, we decided to perform DEGs analysis of RNA-seq data comparing only PDT with PDT+ATRA. By this, we were able to identify candidate genes and key pathways associated with the synergistic effect between ATRA and PDT in HT-29 cells. Based on Prasmickaite *et al*. [24], RNA was harvested 3 hours post-light exposure using a photochemical light dose corresponding to ~ LD_{50}. We identified 1129 genes that were significantly differentially expressed; 676 genes (59.9%) upregulated and 453 (40.1%) downregulated (**Supplementary Table S1**). Among the significant DEGs, 103 genes showed a log2-fold change of at least 1 (**Supplementary Table S2**) including, 56 upregulated (54.4%) and 47 downregulated (45.6%) (**Fig. 3a**). The sequencing data are deposited at the European Nucleotide Archive (ENA, https://www.ebi.ac.uk/ena) with the study number PRJEB49953.

Gene set enrichment analysis (GSEA)

To obtain specific, well-defined biological states or processes underlying ATRA+PDT, all significant DEGs were first submitted to the GSEA software using the MSigDB hallmark gene set collection. The analysis revealed ten significantly enriched gene sets (**Fig. 3b**). Interestingly, a significant enrichment in immune-related gene sets were identified (allograft rejection, inflammation, and IFN-α/ IFN-γ response). Moreover, apoptosis and upregulation of KRAS signaling were positively correlated to ATRA+PDT, whereas late estrogen response, fatty acid metabolism, and xenobiotic metabolism were negatively correlated.

All significant DEGs were further analyzed using the Ingenuity Pathway Analysis (IPA) software for gene set enrichment analysis to gain mechanistic insight into the data on biological processes, pathways, molecular networks, and upstream regulators. The IPA results revealed that 68 canonical pathways were significantly enriched, of which 12 pathways had a

significant activation z-score (**Supplementary Table S3**). Five canonical pathways were significantly activated, and seven were predicted to be significantly inhibited (**Fig. 3c).** Strikingly, the UPR (**Fig. 3d**), IFN signaling and retinoic acid-mediated apoptosis signaling were predicted as strongly activated canonical pathways. Although we show that ATRA alone does not induce apoptosis, the ATRA-related genes CRABP2 and RARγ (**Supplementary Fig. S5a)** are mapped to this pathway together with genes involved in apoptosis in IPA (**Supplementary Table S3**). Superpathway of cholesterol biosynthesis and Huntington's disease signaling were predicted as inhibited. Furthermore, top molecular and cellular functions identified by IPA were associated with cellular movement, cell death and survival, cellular development, cellular growth and proliferation, and cell-to-cell signaling interaction.

The upstream regulator analysis (URA) identified 1407 significant regulators ($p \leq 0.01$), of which 229 were predicted as activated and 79 as inhibited (**Supplementary Table 4, Fig. 3c**). Of relevance, strong activation of the pro-inflammatory and immune-related regulators tumor necrosis factor (TNF), lipopolysaccharide (LPS), interferon-gamma (IFNG), poly rI:rC-RNA (a synthetic dsRNA analogue known as poly (I:C)), and interferon-alpha (IFNA) were predicted by the URA. As expected, the upstream regulator tretinoin (ATRA) had a significant activation score (**Fig. 3c**).

Validation of gene expression by quantitative real-time PCR (qRT-PCR)

Quantitative RT-PCR was used to validate the RNA-seq data, including the following 6 DEGs: *REG4* (Regenerating islet-derived protein 4), *IGFBP6* (Insulin-like growth factor-binding protein 6), *ATF3* (Activating transcription factor 3), *EGR1* (Early growth response 1), *LCN2* (Lipocalin 2), and *ALDH1A1* (Aldehyde dehydrogenase 1 family member A1). The

qRT-PCR data revealed that the selected genes' fold-change was comparable to the RNA-sequencing results (**Fig. 4a**)

ATRA+PDT rapidly induces ATF3 and EGR1 expression

ATRA+PDT-treated samples were evaluated using qRT-PCR at 3 and 6 hours post-treatment and compared with non-treated, PDT- and ATRA-treated cells. IGFBP6 and ALDH1A1 have previously been described in the context of ATRA [25, 26], whereas REG4, ATF3, and EGR1 have, to the best of our knowledge, not been associated with ATRA treatment. ATF3 and EGR1 were selected based on their association identified by the STRING network analysis (**Fig. S5b**). Both the ATF3 and EGR1 gene expressions were upregulated synergistically after ATRA+PDT. At 3 hours post-treatment, the EGR1 expression in the non-treated, PDT-, and ATRA-treated samples were comparable (~ 1-fold). ATRA+PDT 3 hours post-treatment induced a 2.5-fold increase in EGR1 expression. The ATF3 level in ATRA-treated cells was comparable to non-treated control, whereas PDT induced a 63-fold increase 3 hours post-light. Remarkably, a 282-fold increase of ATF3 expression was observed 3 hours post-ATRA+PDT. This observation is in line with the literature, which indicates that ATF3 gene expression is rapidly upregulated by various stress signals [27]. The mRNA expression of ATF3 and EGR1 were strongly downregulated 6 hours post-PDT or -ATRA+PDT **(Fig. 4b)**. As expected, no difference in expression of LCN2, ALDH1A1, or IGFBP6 was observed between ATRA and ATRA+PDT at 3 and 6 hours post-light. Strikingly, the REG4 expression was entirely abolished in ATRA- or ATRA+PDT-treated cells, an observation that, to the best of our knowledge, has not been reported before. The increased ATF3 and EGR1 expressions were identified as unique for the ATRA+PDT combination.

The ATF3 protein expression was further validated by Western blotting of PDT- or ATRA+PDT-treated samples 3 and 6 hours post-light exposure (**Fig. 4c**). At the 24 hour time-point, the ATF3 expression was strongly downregulated, with slightly higher ATF3 expression in the ATRA+PDT samples compared to PDT. The basal level of ATF3 was low in the non-treated samples and after ATRA monotherapy (**Fig 4c**).

PDT+ATRA induces initial tumor growth delay and CRs in HT-29 xenografts

The anti-tumor activities of ATRA+PDT were assessed in HT-29 xenografts in athymic nude mice using a systemic protocol and a 652 nm laser dose of 15 J/cm^2. The ATRA+PDT treatment had an initial strong anti-tumor effect; however, due to unexpected adverse effects including, morbidity/mortality of the combination, the ATRA+PDT treatment group size was too small to draw any conclusions (**Supplementary Results**). When a primary lesion or its metastases are accessible, intratumoral (i.t.) injection of anti-cancer drugs, in particular, immunostimulatory agents have been recommended [28]. The treatment protocol was therefore changed to an intratumoral drug-injection strategy, and we also reduced the laser dose to 10 J/cm^2 to achieve a more favorable adverse-effect profile.

In the second modified protocol, both ATRA and fimaporfin ($TPCS_{2a}$) were injected i.t. as a single dose one day (18-24 hours) before light exposure. As anticipated, compared to systemic delivery, i.t. caused only mild adverse effects including, edema and erythema in tumor areas after PDT or ATRA+PDT **(Fig. 5a)**. All ATRA+PDT-treated animals (5/5) had an initial tumor growth delay compared to the other treatment groups (**Fig. 5b-c, Supplementary Fig. S7a**). By comparing the mean tumor size in each treatment group at 5, 10, and 20 days post-treatment, ATRA+PDT significantly inhibited tumor growth up to 20 days post-treatment compared to non-treated (NT). The mean tumor volume in the ATRA+PDT group was 2-3

times smaller compared to the other treatment groups (not significant) (**Fig. 5b**). Although not reflected in the tumor measurements, visual examination of the PDT- or ATRA+PDT-treated tumors indicated they were flatter or had a necrotic center (**Fig. 5a**). The tumor volume measurements are based on the assumption that tumors are spherical. As the PDT- and ATRA+PDT-treated tumors are not spherical (but flat with a necrotic core), these groups' tumor measurements are most likely overestimated. During laser illumination, fluorescence was observed in tumors injected with fimaporfin ($TPCS_{2a}$) alone or in combination with ATRA (ATRA+PDT) (**Fig. 5d**). In the PDT group, the fluorescence was limited to the tumor, indicating that most of the photosensitizer is confined in the tumor. Intriguingly, in the ATRA+PDT group, fluorescence in the tumor margin could also be observed.

Two out of five (40%) ATRA+PDT-treated animals achieved complete responses (CR) after only one treatment (**Fig. 5e**). However, one of the cured animals was euthanized on day 21 due to weight loss, probably not associated with the treatment as one animal in the NT group was also euthanized due to weight loss (**Fig. 5f**). None of the mice in any of the other treatment groups achieved CR. The animals were followed up to at least 90 days post-treatment. Surprisingly, in the ATRA group, 3/5 animals reached day 90 post-treatment. The ATRA-treated tumors grew similar to the controls up to 20 days post-treatment. However, tumor growth stagnated over time (**Supplementary Fig. S7b**), and surprisingly, the best overall survival was obtained with ATRA monotherapy ($p = 0.012$ compared to NT (**Fig. 5c**). The mean time to reach the endpoint (day 90, weight loss ≥ 20% and/or tumor size ≥ 1000 mm^3) was longest in the ATRA group (76.8 ± 8.1 days) (**Supplementary Fig. S7c**).

As the impact of the needle trauma and injection of fluids on the tumor microenvironment was unknown, a sham procedure including an i.t. injection of PBS was included in addition to

the NT control group. No animals in the NT group reached day 90. However, 2/5 animals in the PBS treatment group reached day 90, of which one animal was at endpoint (tumor volume >1000 mm^3) (**Supplementary Fig. S7d**). The fact that PBS-treated animals also survived up to day 90 indicates that i.t. injection of fluids itself affects tumor growth. One of five animals in the PDT group (tumor volume >1000 mm^3) and in the ATRA+PDT group (CR) also reached day 90 (**Supplementary Fig. S7d**).

Discussion

ATRA has not proven successful in the treatment of solid tumors due to intrinsic or acquired drug resistance. It is therefore suggested that ATRA needs to be combined with other therapies to improve therapeutic outcomes [4]. In this study, we present evidence demonstrating that ATRA preconditioning combined with fimaporfin-PDT (ATRA+PDT) is a promising anti-carcinoma strategy. Different experiments were conducted to identify the possible mechanism behind the enhanced efficacy of ATRA+PDT, including assessment of differentiation, ROS-generation, mTOR inhibition, cell cycle distribution, and cytotoxic products of ATRA and fimaporfin, of which none were identified as the mechanism. Thus, in an effort to provide a mechanistic rationale for how ATRA preconditioning is able to enhance the cytotoxic efficacy of PDT, we decided to determine the differences of gene expression levels between the two experimental conditions PDT and ATRA+PDT by RNA-seq. DEG analysis of the RNA-seq data revealed a complex transcriptome profile post-ATRA+PDT. The DEG analysis indicated that EGR1 and ATF3 were significantly upregulated in ATRA+PDT-treated cells. In line with our observation, the stress response transcription regulator ATF3 has previously shown to be induced after PDT [24, 29, 30], and implicated in the UPR [31]. ATF3 was therefore selected for further analysis and validation on the mRNA and protein level. Strikingly, the qRT-PCR results indicated a 282- and 63-fold increase in

ATF3 mRNA in the ATRA+PDT- and PDT-treated cells, respectively. Increased ATF3 protein expression after ATRA+PDT was also confirmed.

The IPA bioinformatics analysis revealed pathways and upstream regulators supporting our observation related to enhanced cytotoxicity of ATRA+PDT, including apoptosis and the UPR as one of the top pathways. Misfolded protein or the formation of protein aggregates due to ROS-induced proteotoxic stress is a primary response to PDT independent of the cell type and PDT strategy [32]. Upon endoplasmic reticulum (ER) stress, UPR is activated to reduce accumulation and aggregation of misfolded or unfolded proteins playing an important role in homeostasis and cell survival. However, if the ER stress is excessive and sustained, apoptosis is induced [33]. Indeed, our observation of ATRA+PDT-enhanced apoptotic cell death by the TUNEL assay was supported by both GSEA and IPA. Western blot analysis indicated increased cleaved caspase-3 post-ATRA+PDT, but not significantly elevated compared to PDT, which was confirmed by the DEG-analysis. However, compared to PDT monotherapy, DEG-analysis revealed significant upregulation of caspase-4, -7, and -9 post-ATRA+PDT. Furthermore, TNF-α, a potent pro-apoptotic trigger that may also induce necrosis [34], was identified as an activated upstream regulator after ATRA+PDT [34].

Interestingly, the downstream effects of the p38 kinase inhibitor SB203580 were predicted to be significantly inhibited suggesting that p38 kinase is involved in stress-induced death signalling after ATRA+PDT. This is consistent with previous observations; Weyergang *et al.* demonstrated that SB203580 in combination with $TPPS_{2a}$-based PDT resulted in increased cell viability [35], while similar effects were shown by Olsen *et al.* where SB203580 was combined with fimaporfin-PDT [21].

Of notice, HDAC was identified as one of the upstream regulators with a negative z-score indicating HDAC inhibition (HDACi) despite that the class II deacetylase HDAC9 was 2.2-fold upregulated by ATRA+PDT. HDAC9 negatively regulates the function of TRIM29 by non-histone deacetylation of the protein [36], and thereby alters its ability to associate with p53 and consequently inhibits its cell proliferation-promoting activity. Interestingly, our RNA-seq data reveal that TRIM29 is 30% downregulated post-ATRA+PDT (p = 5.00E-05), which may strengthen the concept of the HDACi effect of ATRA+PDT.

The ATRA+PDT combination strategy was further evaluated *in vivo* by using the HT-29 xenograft model in athymic nude mice. High morbidity (significant weight loss and xeroderma) was observed when ATRA was combined with $TPCS_{2a}$-PDT systemically. In an effort to enhance the safety profile and anti-tumor efficacy, ATRA and $TPCS_{2a}$ were co-administered i.t. This technique was recently suggested by Marabelle *et al.* as a strategy to deliver immunostimulatory agents [28]. This strategy also offers high drug concentration in the tumor and has previously been explored by us using ribosome-inactivating protein toxins, in combination with an amphiphilic photosensitizer that was delivered systemically [37, 38].

Remarkably, 40% (2/5) of the ATRA+PDT-treated animals achieved CR after only one treatment, whereas no CRs were obtained in the other treatment groups. Moreover, all ATRA+PDT-treated animals had significantly smaller tumors than NT during the first 20 days post-treatment. In the ATRA+PDT group, fimaporfin fluorescence was observed in the tumors as well as in the tumor margins during light exposure, as opposed to the PDT treatment group, where the fluorescence was confined to the tumors only. Although the exact mechanism of this ATRA effect is not clear, the enhanced $TPCS_{2a}$ distribution in the tumor margin may contribute to the improved overall PDT response and explain the initial tumor

growth inhibition in the ATRA+PDT group. In addition to direct cell killing, PDT with PCI-based photosensitizers also targets the tumor vasculature [39-41]. Thus, light activation of fimaporfin in the tumor periphery of the ATRA+PDT-treated animals may induce vascular shutdown, which limits the oxygen and nutrition supply to the tumor, but this remains to be tested experimentally. Despite the CRs obtained after ATRA+PDT, ATRA monotherapy surprisingly gave the best overall survival, of which 60% of the mice were still alive at day 90.

In conclusion, our study shows that ATRA preconditioning is a promising strategy to improve the efficacy of PDT in carcinomas and identify enhanced activation of apoptosis as a death mechanism. DEG analysis predicted the unfolded protein response as the most significantly upregulated pathway. To fully exploit the potential of this preconditioning approach, preclinical studies of ATRA in combination with laser-activation of the clinical relevant photosensitizer fimaporfin (PDT or PCI) in immunocompetent murine models are warranted.

Materials and Methods

Cell lines

All the cell lines were purchased from American Type Culture Collections (ATCC, Manassas, VA, USA), except the MC-38 cell line, which was from Kerafast (Boston, MA, USA). A detailed description of the cell lines and culture conditions are detailed in **Supplementary Materials and Methods**.

Drugs and chemicals

ATRA (Sigma-Aldrich, Saint-Louis, MO, USA) was dissolved in DMSO was stored at -80 °C. The photosensitizer $TPCS_{2a}$ (in polysorbate 80, 2.8% mannitol, 50 mM Tris, pH 8.5) was

provided by PCI Biotech AS (Oslo, Norway) and stored at 4 °C. All work with ATRA or $TPCS_{2a}$ was performed under subdued light.

***In vitro* ATRA+PDT treatment protocol**

To evaluate the treatment effects of ATRA+PDT, 3000 (HCT116 and HT-29) or 8000 (SKBR3) cells/well were seeded in 96-well plates (Nunc). The cells were first incubated with 0.1 µM ATRA for 24 hours and further incubated with 0.1 µM ATRA and/or 0.4 µg/mL $TPCS_{2a}$ for 18 hours. Before light exposure, the cells were washed twice with PBS, chased for 4 hours in fresh media, and illuminated with LumiSource (PCI Biotech, Oslo, Norway) [41]. Cell viability was evaluated 48 hours post-treatment. The treatment protocol for MC-38 and MDA-MB-231 is described in **Supplementary Materials and Methods**.

Evaluation of treatment-induced cytotoxicity and effect on proliferation

A description of the MTT assay, clonogenic assay, and the real-time monitoring of cell proliferation can be found in **Supplementary Materials and Methods.**

Apoptosis and cell cycle analysis

The TUNEL assay and cell cycle analyses were performed as previously described [21] and detailed in **Supplementary Materials and Methods**.

Detection of intracellular ROS

The cell permeant reagent 2’,7’-dichlorofluorescin diacetate (DCF-DA) and its downstream product 2’,7’-dichlorofluorescein (DCF) was used to quantitatively assess ROS by flow cytometry in live cell samples as previously described [21].

Flow cytometry

Flow cytometry was performed using an LSRII flow cytometer (Becton Dickinson, Franklin Lakes, NJ, USA). Data were processed using the FlowJo software version 10 (Treestar, OR, USA).

RNA extraction and qRT-PCR

Total cellular RNA was extracted from HT-29 cells at indicated time-points after treatments prior to qRT-PCR as detailed in **Supplementary Materials and Methods**.

Western blot analysis

Western blot was performed as previously described [42] and detailed in **Supplementary Materials and Methods**.

RNA-seq and differential gene analysis

Total RNA was isolated from three biological replicates of HT-29 cells treated with PDT or ATRA+PDT. The samples were harvested 3 hours post-120 seconds blue light exposure, which corresponds to ~LD_{50} measured by MTT. The RNA integrity number (RIN) was evaluated using the 2100 Bioanalyzer (Agilent Technologies, Santa Clara, CA, USA), where all the samples had a RIN=10. Total RNA (500 ng) was processed using a TruSeq Stranded mRNA kit (Illumina, San Diego, CA, USA) following the manufacturer's recommended procedures. Final libraries were quality controlled using qRT-PCR and pooled. Pooled libraries were sequenced on the NextSeq500 instrument (Illumina) with a HighOutput flow cell, single read sequencing of 75 bp read length, and dual-indexes (IDT UDI's 2x8 bp). For data analysis, FASTQ files were mapped using Star2 aligner (STAR v2.5.0b) and human

reference hg19. Counting, normalization, and differential gene expression analysis were performed using Cufflinks2 (v2.2.1).

Gene set enrichment analyses

Broad Institute's GSEA software 4.1.0 was used to determine whether an *a priori* defined set of genes is represented as DEGs in ATRA+PDT compared to PDT [43, 44]. The Hallmark Gene sets were obtained from the Molecular Signature Database (MSigDb v7.4) [45]. False discovery rate (FDR) of ≤ 25% and p-value ≤ 0.05 was considered significant. Further analysis was performed using the IPA software (Qiagen, Hilden, Germany), which identify canonical pathways and biological functions or diseases significantly associated with the identified DEGs. The IPA software was used to analyze upstream regulators that are predicted to be relevant for the biological mechanisms underlying the data based on information gathered in the literature [46]. An overlap of p-value ≤ 0.01 and an activation z-score ≥ |2| was considered significant. The z-score is used to deduce likely activation states based on significant pattern matches of up- or downregulated genes. A positive z-score predicts activation, and a negative z-score indicates inhibition.

Animal studies

All animal procedures were performed according to protocols approved by the Norwegian Food Safety Authority, which is the national animal research authority, and were conducted according to the Federation of European Laboratory Animal Science Association (FELASA) regulations. A detailed description can be found in **Supplementary Materials and Methods.**

Statistical Analysis

Statistical analyses were performed using SigmaPlot 14.0 (Systat Software, Inc., San Jose, CA, USA). Statistical significance was set at $p \leq 0.05$ unless stated otherwise. Synergy was evaluated by comparing the difference in log (DL) of the calculated additive effect with the observed effect, as previously described [47]. Survival analysis was performed by pairwise log-rank (Mantel-Cox) comparison using SPSS Statistics 26 (IBM, Armonk, NY, USA).

Author Contributions: J.J.W.W. planned, performed, analyzed almost all experiments. J.J.W.W. prepared the samples for RNA-seq. S.L. was involved in planning the RNA-seq experiments, performed, and analyzed the RNA-seq data, and contributed to the gene set enrichment analysis interpretation. J.J.W.W. and P.K.S. planned and performed the animal studies. J.J.W.W. and P.K.S. wrote the manuscript with input from S.L. P.K.S. conceived the original idea, acquired funding, provided resources, and supervised the project.

Funding: This research was funded by the South-Eastern Norway Regional Health Authority (Helse-Sør Øst) (grant number: 2017068 (P.K.S.) and 2016023 (J.J.W.W.)) and The Norwegian Radium Hospital Research Foundation (funding number: FU0803 (P.K.S.)).

Acknowledgments: We thank Drs. Trond Stokke and Idun Dale Rein at the Flow Cytometry Core facility for advice on cell cycle analysis. We also thank Ane Sager Longva for excellent technical assistance and advice on RNA extraction, qRT-PCR and Western blotting. We also acknowledge Miriam Rosvold From for great assistance on the MDA-MB-231 cell experiments and Ane Sofie Fremstedal for processing the tumor measurement data.

Conflicts of Interest: P.K.S. and J.J.W.W. has filed a patent (US 63/282,267 (2021)) on the ATRA+PDT method. P.K.S. is a co-inventor on several patents and patent applications related to the PCI technology. S.L. declares no conflict of interest.

References

1. Tang XH, Gudas LJ: Retinoids, retinoic acid receptors, and cancer. *Annu Rev Pathol* 2011, 6:345-364.
2. Altucci L, Leibowitz MD, Ogilvie KM, de Lera AR, Gronemeyer H: RAR and RXR modulation in cancer and metabolic disease. *Nat Rev Drug Discov* 2007, 6(10):793-810.
3. Thomas X: Acute Promyelocytic Leukemia: A History over 60 Years-From the Most Malignant to the most Curable Form of Acute Leukemia. *Oncol Ther* 2019, 7(1):33-65.
4. Ferreira R, Napoli J, Enver T, Bernardino L, Ferreira L: Advances and challenges in retinoid delivery systems in regenerative and therapeutic medicine. *Nat Commun* 2020, 11(1):4265.
5. Muindi JR, Frankel SR, Huselton C, DeGrazia F, Garland WA, Young CW, Warrell RP, Jr.: Clinical pharmacology of oral all-trans retinoic acid in patients with acute promyelocytic leukemia. *Cancer Res* 1992, 52(8):2138-2142.
6. Connolly RM, Nguyen NK, Sukumar S: Molecular pathways: current role and future directions of the retinoic acid pathway in cancer prevention and treatment. *Clin Cancer Res* 2013, 19(7):1651-1659.
7. Duong V, Rochette-Egly C: The molecular physiology of nuclear retinoic acid receptors. From health to disease. *Biochim Biophys Acta* 2011, 1812(8):1023-1031.
8. Agostinis P, Berg K, Cengel KA, Foster TH, Girotti AW, Gollnick SO, Hahn SM, Hamblin MR, Juzeniene A, Kessel D *et al*: Photodynamic therapy of cancer: an update. *CA Cancer J Clin* 2011, 61(4):250-281.

9. Ortel B, Sharlin D, O'Donnell D, Sinha AK, Maytin EV, Hasan T: Differentiation enhances aminolevulinic acid-dependent photodynamic treatment of LNCaP prostate cancer cells. *Br J Cancer* 2002, 87(11):1321-1327.

10. Selbo PK, Weyergang A, Hogset A, Norum OJ, Berstad MB, Vikdal M, Berg K: Photochemical internalization provides time- and space-controlled endolysosomal escape of therapeutic molecules. *J Control Release* 2010, 148(1):2-12.

11. Sultan AA, Jerjes W, Berg K, Hogset A, Mosse CA, Hamoudi R, Hamdoon Z, Simeon C, Carnell D, Forster M *et al*: Disulfonated tetraphenyl chlorin (TPCS2a)-induced photochemical internalisation of bleomycin in patients with solid malignancies: a phase 1, dose-escalation, first-in-man trial. *Lancet Oncol* 2016, 17(9):1217-1229.

12. Otterhaug T, Janetzki S, Welters MJP, Hakerud M, Nedberg AG, Edwards VT, Boekestijn S, Loof NM, Selbo PK, Olivecrona H *et al*: Photochemical Internalization Enhanced Vaccination Is Safe, and Gives Promising Cellular Immune Responses to an HPV Peptide-Based Vaccine in a Phase I Clinical Study in Healthy Volunteers. *Front Immunol* 2020, 11:576756.

13. Trojan J, Hoffmeister A, Neu B, Kasper S, Dechêne A, Jürgensen C, Schirra J, Jakobs R, Palmer D, Selbo P *et al*: Photochemical Internalization of Gemcitabine Is safe and Effective in Locally Advanced Inoperable Cholangiocarcinoma. *The Oncologist* 2022, In press.

14. Jing J, Isoherranen N, Robinson-Cohen C, Petrie I, Kestenbaum BR, Yeung CK: Chronic Kidney Disease Alters Vitamin A Homeostasis via Effects on Hepatic RBP4 Protein Expression and Metabolic Enzymes. *Clin Transl Sci* 2016, 9(4):207-215.

15. Adamson PC, Bailey J, Pluda J, Poplack DG, Bauza S, Murphy RF, Yarchoan R, Balis FM: Pharmacokinetics of all-trans-retinoic acid administered on an intermittent schedule. *J Clin Oncol* 1995, 13(5):1238-1241.

16. Lee MO, Han SY, Jiang S, Park JH, Kim SJ: Differential effects of retinoic acid on growth and apoptosis in human colon cancer cell lines associated with the induction of retinoic acid receptor beta. *Biochem Pharmacol* 2000, 59(5):485-496.

17. Paroni G, Fratelli M, Gardini G, Bassano C, Flora M, Zanetti A, Guarnaccia V, Ubezio P, Centritto F, Terao M *et al*: Synergistic antitumor activity of lapatinib and retinoids on a novel subtype of breast cancer with coamplification of ERBB2 and RARA. *Oncogene* 2012, 31(29):3431-3443.

18. Liu RZ, Graham K, Glubrecht DD, Germain DR, Mackey JR, Godbout R: Association of FABP5 expression with poor survival in triple-negative breast cancer: implication for retinoic acid therapy. *Am J Pathol* 2011, 178(3):997-1008.

19. Ronan T. Swords P, Tino Schenk, Sven Stengel, Veronica Sylvina Gil, Kevin R. Petrie, Aymee Perez, Rodriguez Ana, Justin M. Watts, Fernando Vargas, Roy Elias and Arthut Zelent: Inhibition of the PI3K/AKT/mTOR Pathway Leads to Down-Regulation of c-Myc and Overcomes Resistance to ATRA in Acute Myeloid Leukemia. *Blood* 2015, 126(23):1363.

20. Bostad M, Olsen CE, Peng Q, Berg K, Hogset A, Selbo PK: Light-controlled endosomal escape of the novel CD133-targeting immunotoxin AC133-saporin by photochemical internalization - A minimally invasive cancer stem cell-targeting strategy. *J Control Release* 2015, 206:37-48.

21. Olsen CE, Weyergang A, Edwards VT, Berg K, Brech A, Weisheit S, Hogset A, Selbo PK: Development of resistance to photodynamic therapy (PDT) in human breast cancer cells is photosensitizer-dependent: Possible mechanisms and approaches for overcoming PDT-resistance. *Biochem Pharmacol* 2017, 144:63-77.

22. Mathieu J, Giraudier S, Lanotte M, Besancon F: Retinoid-induced activation of NF-kappaB in APL cells is not essential for granulocytic differentiation, but prolongs the life span of mature cells. *Oncogene* 2005, 24(48):7145-7155.

23. Shin J, Carr A, Corner GA, Togel L, Davalos-Salas M, Tran H, Chueh AC, Al-Obaidi S, Chionh F, Ahmed N *et al*: The intestinal epithelial cell differentiation marker intestinal alkaline phosphatase (ALPi) is selectively induced by histone deacetylase inhibitors (HDACi) in colon cancer cells in a Kruppel-like factor 5 (KLF5)-dependent manner. *J Biol Chem* 2014, 289(36):25306-25316.

24. Prasmickaite L, Cekaite L, Hellum M, Hovig E, Høgset A, Berg K: Transcriptome changes in a colon adenocarcinoma cell line in response to photochemical treatment as used in photochemical internalisation (PCI). *FEBS Letters* 2006, 580(24):5739-5746.

25. Kim EJ, Kang YH, Schaffer BS, Bach LA, MacDonald RG, Park JH: Inhibition of Caco-2 cell proliferation by all-trans retinoic acid: role of insulin-like growth factor binding protein-6. *J Cell Physiol* 2002, 190(1):92-100.

26. Bhatlekar S, Viswanathan V, Fields JZ, Boman BM: Overexpression of HOXA4 and HOXA9 genes promotes self-renewal and contributes to colon cancer stem cell overpopulation. *J Cell Physiol* 2018, 233(2):727-735.

27. Hai T, Wolford CC, Chang YS: ATF3, a hub of the cellular adaptive-response network, in the pathogenesis of diseases: is modulation of inflammation a unifying component? *Gene Expr* 2010, 15(1):1-11.

28. Marabelle A, Andtbacka R, Harrington K, Melero I, Leidner R, de Baere T, Robert C, Ascierto PA, Baurain JF, Imperiale M *et al*: Starting the fight in the tumor: expert recommendations for the development of human intratumoral immunotherapy (HIT-IT). *Ann Oncol* 2018, 29(11):2163-2174.

29. Cekaite L, Peng Q, Reiner A, Shahzidi S, Tveito S, Furre IE, Hovig E: Mapping of oxidative stress responses of human tumor cells following photodynamic therapy using hexaminolevulinate. *BMC Genomics* 2007, 8:273.

30. Weijer R, Broekgaarden M, van Golen RF, Bulle E, Nieuwenhuis E, Jongejan A, Moerland PD, van Kampen AH, van Gulik TM, Heger M: Low-power photodynamic therapy induces survival signaling in perihilar cholangiocarcinoma cells. *BMC Cancer* 2015, 15:1014.

31. Jiang HY, Wek SA, McGrath BC, Lu D, Hai T, Harding HP, Wang X, Ron D, Cavener DR, Wek RC: Activating transcription factor 3 is integral to the eukaryotic initiation factor 2 kinase stress response. *Mol Cell Biol* 2004, 24(3):1365-1377.

32. Broekgaarden M, Weijer R, van Gulik TM, Hamblin MR, Heger M: Tumor cell survival pathways activated by photodynamic therapy: a molecular basis for pharmacological inhibition strategies. *Cancer Metastasis Rev* 2015, 34(4):643-690.

33. Hetz C: The unfolded protein response: controlling cell fate decisions under ER stress and beyond. *Nat Rev Mol Cell Biol* 2012, 13(2):89-102.
34. Chu WM: Tumor necrosis factor. *Cancer Lett* 2013, 328(2):222-225.
35. Weyergang A, Kaalhus O, Berg K: Photodynamic therapy with an endocytically located photosensitizer cause a rapid activation of the mitogen-activated protein kinases extracellular signal-regulated kinase, p38, and c-Jun NH2 terminal kinase with opposing effects on cell survival. *Mol Cancer Ther* 2008, 7(6):1740-1750.
36. Yuan Z, Peng L, Radhakrishnan R, Seto E: Histone deacetylase 9 (HDAC9) regulates the functions of the ATDC (TRIM29) protein. *J Biol Chem* 2010, 285(50):39329-39338.
37. Berstad MB, Cheung LH, Berg K, Peng Q, Fremstedal AS, Patzke S, Rosenblum MG, Weyergang A: Design of an EGFR-targeting toxin for photochemical delivery: in vitro and in vivo selectivity and efficacy. *Oncogene* 2015, 34(44):5582-5592.
38. Selbo PK, Sivam G, Fodstad O, Sandvig K, Berg K: In vivo documentation of photochemical internalization, a novel approach to site specific cancer therapy. *Int J Cancer* 2001, 92(5):761-766.
39. Weyergang A, Cheung LH, Rosenblum MG, Mohamedali KA, Peng Q, Waltenberger J, Berg K: Photochemical internalization augments tumor vascular cytotoxicity and specificity of VEGF(121)/rGel fusion toxin. *J Control Release* 2014, 180:1-9.
40. Vikdal M, Weyergang A, Selbo PK, Berg K: Vascular endothelial cells as targets for photochemical internalization (PCI). *Photochem Photobiol* 2013, 89(5):1185-1192.
41. Wong JJW, Berstad MB, Fremstedal ASV, Berg K, Patzke S, Sorensen V, Peng Q, Selbo PK, Weyergang A: Photochemically-Induced Release of Lysosomal Sequestered Sunitinib: Obstacles for Therapeutic Efficacy. *Cancers (Basel)* 2020, 12(2).
42. Berstad MEB, Cheung LH, Weyergang A: Production of Recombinant Gelonin Using an Automated Liquid Chromatography System. *Toxins (Basel)* 2020, 12(8).
43. Mootha VK, Lindgren CM, Eriksson KF, Subramanian A, Sihag S, Lehar J, Puigserver P, Carlsson E, Ridderstrale M, Laurila E *et al*: PGC-1alpha-responsive

genes involved in oxidative phosphorylation are coordinately downregulated in human diabetes. *Nat Genet* 2003, 34(3):267-273.

44. Subramanian A, Tamayo P, Mootha VK, Mukherjee S, Ebert BL, Gillette MA, Paulovich A, Pomeroy SL, Golub TR, Lander ES *et al*: Gene set enrichment analysis: a knowledge-based approach for interpreting genome-wide expression profiles. *Proc Natl Acad Sci U S A* 2005, 102(43):15545-15550.

45. Liberzon A, Birger C, Thorvaldsdottir H, Ghandi M, Mesirov JP, Tamayo P: The Molecular Signatures Database (MSigDB) hallmark gene set collection. *Cell Syst* 2015, 1(6):417-425.

46. Kramer A, Green J, Pollard J, Jr., Tugendreich S: Causal analysis approaches in Ingenuity Pathway Analysis. *Bioinformatics* 2014, 30(4):523-530.

47. Weyergang A, Kaalhus O, Berg K: Photodynamic targeting of EGFR does not predict the treatment outcome in combination with the EGFR tyrosine kinase inhibitor Tyrphostin AG1478. *Photochemical & Photobiological Sciences* 2008, 7(9):1032-1040.

Figure legends

Fig. 1. ATRA preconditioning enhances the cytotoxic efficacy of fimaporfin-PDT and strongly impair proliferation in carcinoma cells.

a Viability assessed by MTT 48 hours post-light exposure in SKBR3, HT-29, and HCT116 cells treated with fimaporfin-PDT or the combination ATRA+PDT. Representative data of at least three independent experiments. Data presented as mean of triplicates ± S.D. 60 seconds light exposure ≈ 0.58 J/cm^2. **b** Synergistic cytotoxic effects induced by ATRA+PDT in HT-29 and SKBR3 cells. The observed effect of the combination in SKBR3 and HT-29 compared to a theoretical additive effect at ~ LD_{60} of at least three independent experiments. Data presented as mean ± S.E. **c** Representative clonogenic assay of PDT compared to ATRA+PDT in HT-29 cells. **d** Proliferation of SKBR3, HT-29 and HCT116 up to 110 hours post-120 seconds light exposure (1.16 J/cm^2). Representative experiment of three experiments, data presented as mean of triplicates ± S.E. Statistical significance calculated using Student's two-tailed t-test (*** $p \leq 0.001$, ** $p \leq 0.01$, * $p \leq 0.05$).

Fig. 2. ATRA preconditioning increases PDT-induced cell cycle arrest and apoptosis

The cells were subjected to 120 seconds (SKBR3) and 90 seconds (HT-29 and HCT116) light exposure, which corresponds to ≈ 1.16 J/cm^2 and 0.87 J/cm^2, respectively. 4 Gy-treated Reh cells harvested 24 hours post-radiotherapy was included as a positive control. **a** Cell cycle analysis at 24- and 72-hours post-light exposure. Left panels, percent distribution in G2/M, S, and G1 phase after the different treatments. Data presented as mean of three independent experiments ± S.E. Right panels, representative cell cycle histograms. **b** Apoptosis was evaluated by the TUNEL assay at 24- and 72-hours post-treatment. Data presented as mean of three experiments ± S.E. **c** Western blot of cleaved caspase-3 in HT-29 cells harvested 72 hours post-treatment. Cells treated with 10 Gy were included as a positive control, and γ-

tubulin was included as a loading control. Representative blot of three experiments. **d** Intracellular ROS was measured using the DCFH-DA assay immediately after light exposure. Data are normalized to non-treated samples and presented as mean of three experiments ± S.E. Statistical significance calculated with one-way ANOVA. (*** $p \leq 0.001$, ** $p \leq 0.01$ and * $p \leq 0.05$, n.s.: not significant).

Fig. 3. Differentially expressed genes (DEGs) and gene set enrichment analyses (GSEA) in ATRA+PDT-treated HT-29 cells compared to PDT-treatment.

a Heat map of DEGs of fold change ≥ |2| at 3 hours post-light exposure in PDT and ATRA+PDT-treated samples. **b** All significantly enriched biological states or processes in ATRA+PDT compared to PDT determined by GSEA analysis using the Hallmark gene set. A p-value of ≤ 0.05 and an FDR of ≤ 25% were considered significant. **c** Visualization of IPA analysis of top five canonical pathways based on p-value, top five molecular and cellular functions, and top ten activated and inhibited based on z-value. A p-value of ≤ 0.01 and a predicted activation, z-score of ≥ |2| were considered significant. **d** Heat map of DEGs mapped to the unfolded protein response.

Fig. 4. Post-RNA-seq validation of six selected DEGs by qRT-PCR and ATF3 protein expression by Western blotting.

a Validation of mRNA expression of six selected DEGs (ALDH1A1, ATF3, EGR1, IGFBP6, LCN2 and REG4) by RT-qPCR of samples harvested 3 hours post-treatment. Quantitative RT-PCR data are presented as log-2-fold change (FC) (ratio of ATRA+PDT/PDT) and compared to the RNA-seq data. **b** Relative normalized expression of DEGs in samples obtained 3 or 6 hours post-ATRA+PDT treatment and compared to non-treated (NT), ATRA- and PDT-treated controls. The data are normalized to two reference genes (RPLP0 and

GADPH) and presented as mean of three experiments ± S.E. Statistical significance calculated with one-way ANOVA. **c** Relative ATF3 signal in ATRA+PDT to PDT samples. The data were normalized to loading control. Data are presented as mean of four experiments ± S.E. One-sample t-test. Representative western blot of ATF3 at 3-, 6-, and 24-hours post-treatment. γ-tubulin was included as a loading control. (*** $p \leq 0.001$, ** $p \leq 0.01$ and * $p \leq 0.05$, n.s.: not significant).

Fig. 5. Treatment response in HT-29 xenograft-tumor bearing mice following i.t. delivery of ATRA and fimaporfin, and photochemical treatment.

a Representative images of one animal in each treatment group at day 0 (before light exposure), 1 and 7 post-treatment. **b** Tumor volume (mm^3) of each treatment group at day 5, 10, and 20 post-treatment. Data presented as mean ± S.E. Statistical significance calculated with one-way ANOVA. (*** $p \leq 0.001$, ** $p \leq 0.01$ and * $p \leq 0.05$, n.s.: not significant)**. c** Tumor growth of individual animals in each treatment group up to 20 days post-treatment. Each line represents one animal. **d** Images of fimaporfin fluorescence in the tumors during light exposure in the PDT- and ATRA+PDT-group. The yellow frames indicate animals that achieved complete responses. **e** Images of the two mice that were cured in the ATRA+PDT group before light exposure (day 0) and post-treatment at a later time-point (day 18 and 102). **f** Relative weight of each individual animal, relative to day -1, in each treatment group. Each line represents one animal. For all treatment groups, n = 5, except for NT where n = 6.

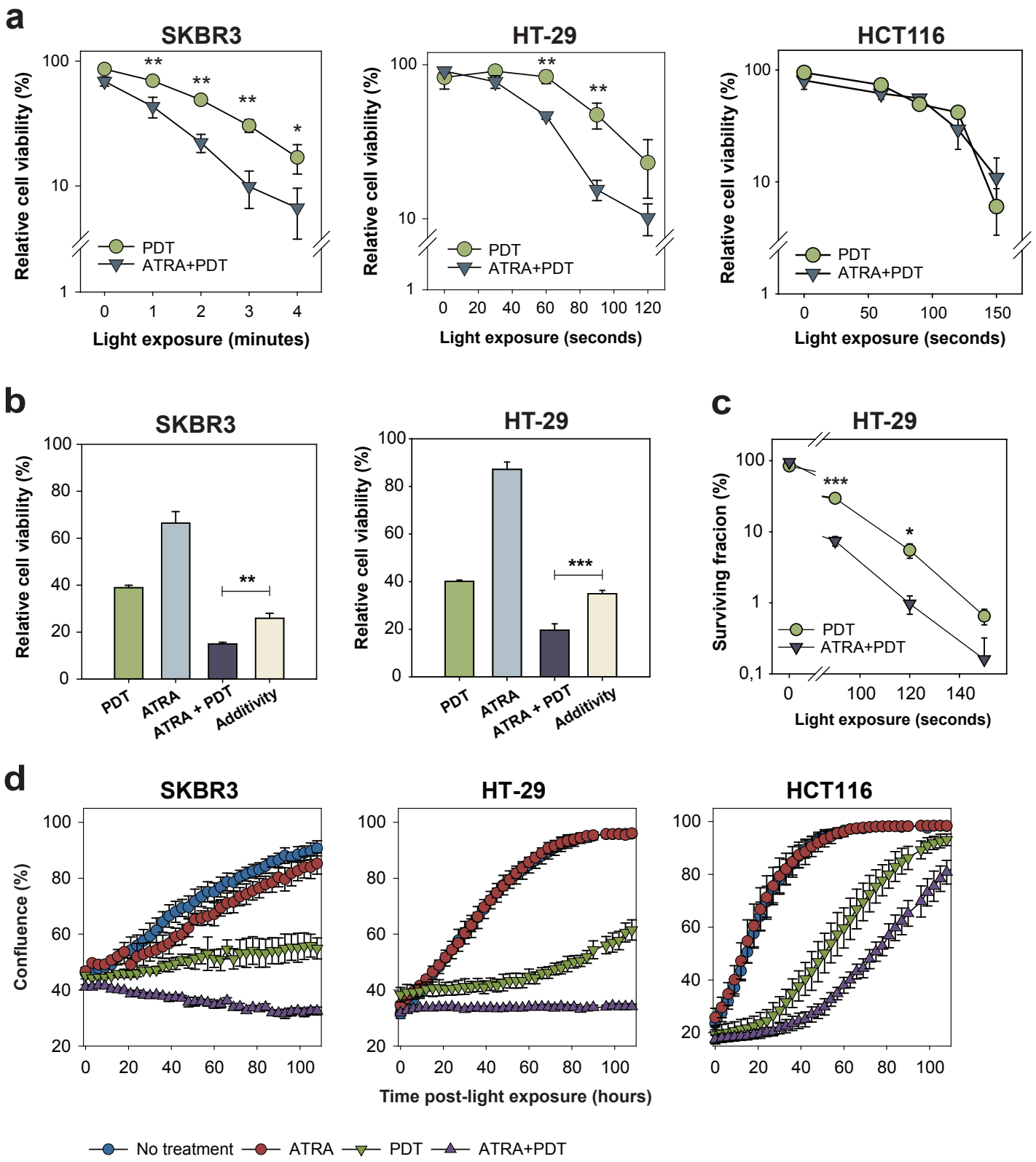
a
SKBR3
HT-29
HCT116
Relative cell viability (%)
PDT
ATRA+PDT
Light exposure (minutes)
Light exposure (seconds)
b
SKBR3
HT-29
Relative cell viability (%)
PDT
ATRA
ATRA + PDT
Additivity
c
HT-29
Surviving fracion (%)
Light exposure (seconds)
d
SKBR3
HT-29
HCT116
Confluence (%)
Time post-light exposure (hours)
No treatment
ATRA
PDT
ATRA+PDT

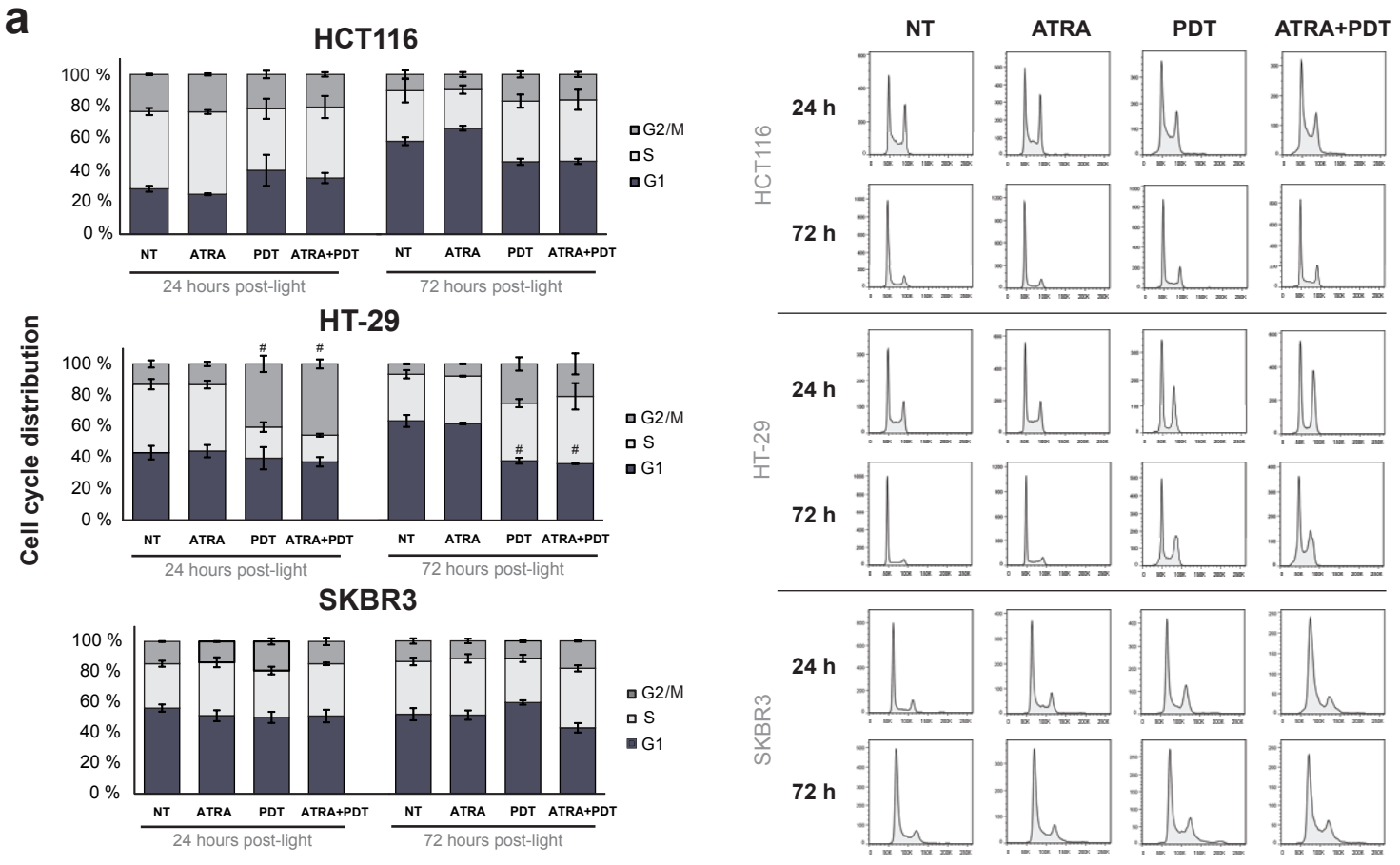
a
HCT116
HT-29
SKBR3
Cell cycle distribution
100 %
80 %
60 %
40 %
20 %
0 %
G2/M
S
G1
NT
ATRA
PDT
ATRA+PDT
24 hours post-light
72 hours post-light
#
NT
ATRA
PDT
ATRA+PDT
24 h
72 h
HCT116
HT-29
SKBR3

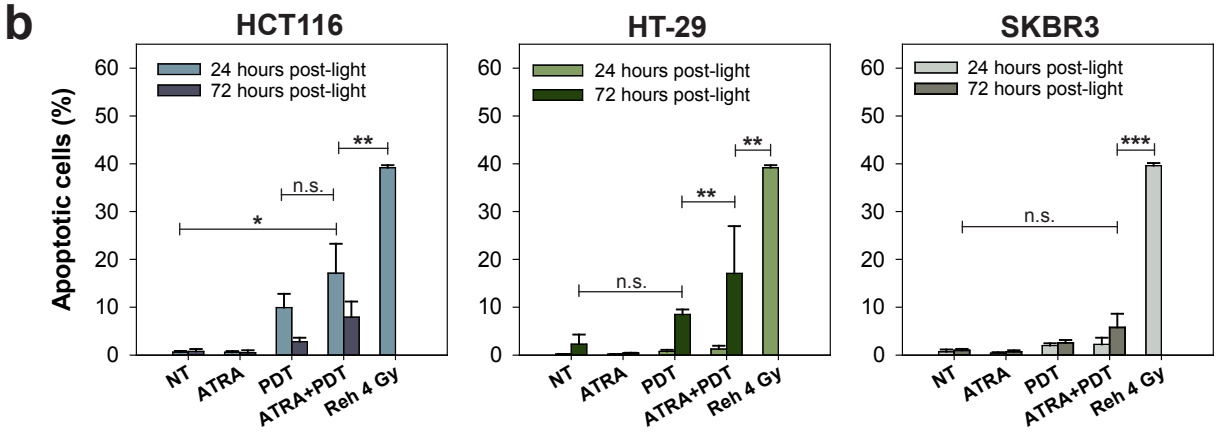
b
HCT116
HT-29
SKBR3
Apoptotic cells (%)
24 hours post-light
72 hours post-light
n.s.
*
**
***
NT
ATRA
PDT
ATRA+PDT
Reh 4 Gy

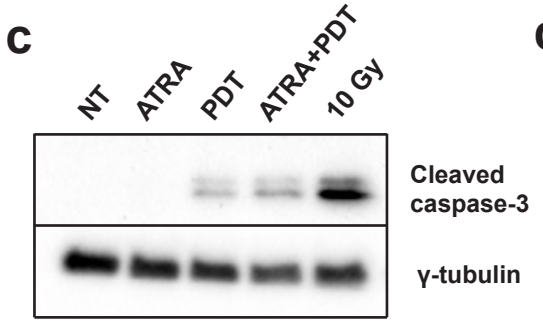
c
NT
ATRA
PDT
ATRA+PDT
10 Gy
Cleaved caspase-3
γ-tubulin

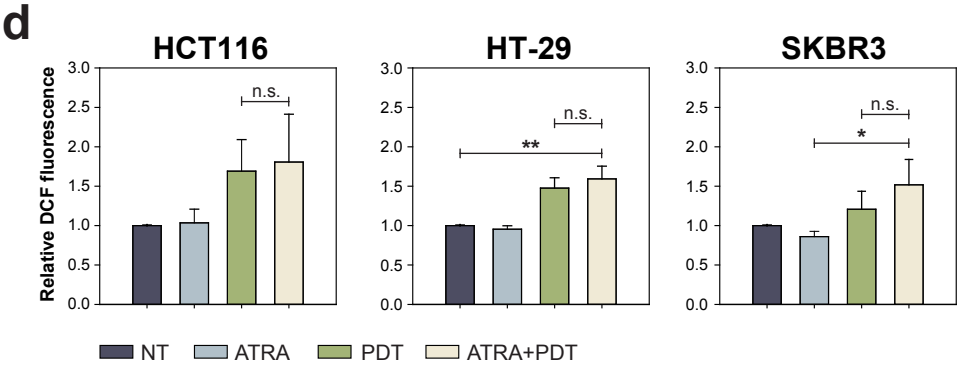
d
HCT116
HT-29
SKBR3
Relative DCF fluorescence
n.s.
*
**
NT
ATRA
PDT
ATRA+PDT

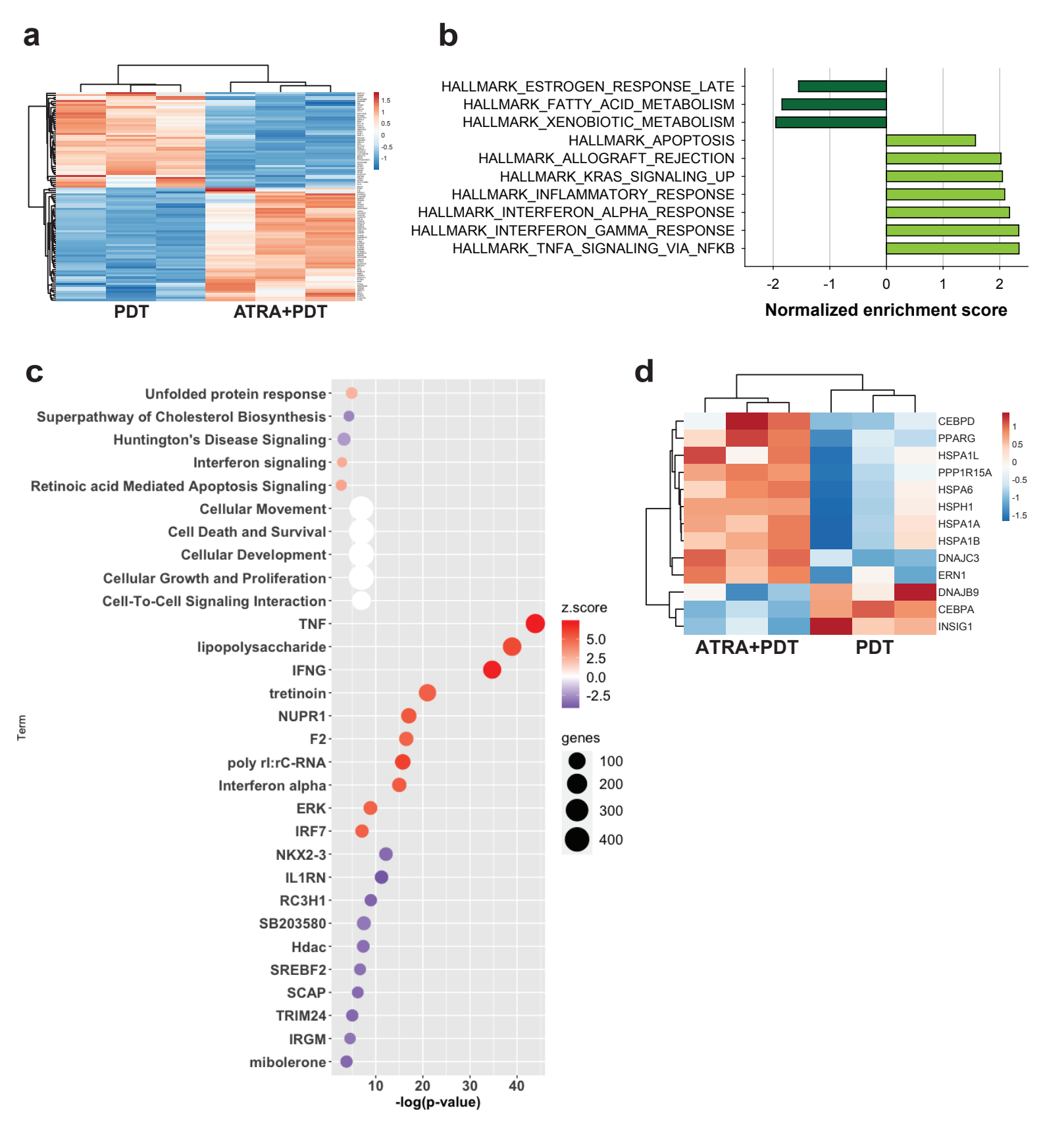
a
1.5
1
0.5
0
-0.5
-1
PDT
ATRA+PDT
b
HALLMARK_ESTROGEN_RESPONSE_LATE
HALLMARK_FATTY_ACID_METABOLISM
HALLMARK_XENOBIOTIC_METABOLISM
HALLMARK_APOPTOSIS
HALLMARK_ALLOGRAFT_REJECTION
HALLMARK_KRAS_SIGNALING_UP
HALLMARK_INFLAMMATORY_RESPONSE
HALLMARK_INTERFERON_ALPHA_RESPONSE
HALLMARK_INTERFERON_GAMMA_RESPONSE
HALLMARK_TNFA_SIGNALING_VIA_NFKB
-2
-1
0
1
2
Normalized enrichment score
c
Unfolded protein response
Superpathway of Cholesterol Biosynthesis
Huntington's Disease Signaling
Interferon signaling
Retinoic acid Mediated Apoptosis Signaling
Cellular Movement
Cell Death and Survival
Cellular Development
Cellular Growth and Proliferation
Cell-To-Cell Signaling Interaction
TNF
lipopolysaccharide
IFNG
tretinoin
NUPR1
F2
poly rI:rC-RNA
Interferon alpha
ERK
IRF7
NKX2-3
IL1RN
RC3H1
SB203580
Hdac
SREBF2
SCAP
TRIM24
IRGM
mibolerone
Term
10
20
30
40
-log(p-value)
z.score
5.0
2.5
0.0
-2.5
genes
100
200
300
400
d
CEBPD
PPARG
HSPA1L
PPP1R15A
HSPA6
HSPH1
HSPA1A
HSPA1B
DNAJC3
ERN1
DNAJB9
CEBPA
INSIG1
1
0.5
0
-0.5
-1
-1.5
ATRA+PDT
PDT

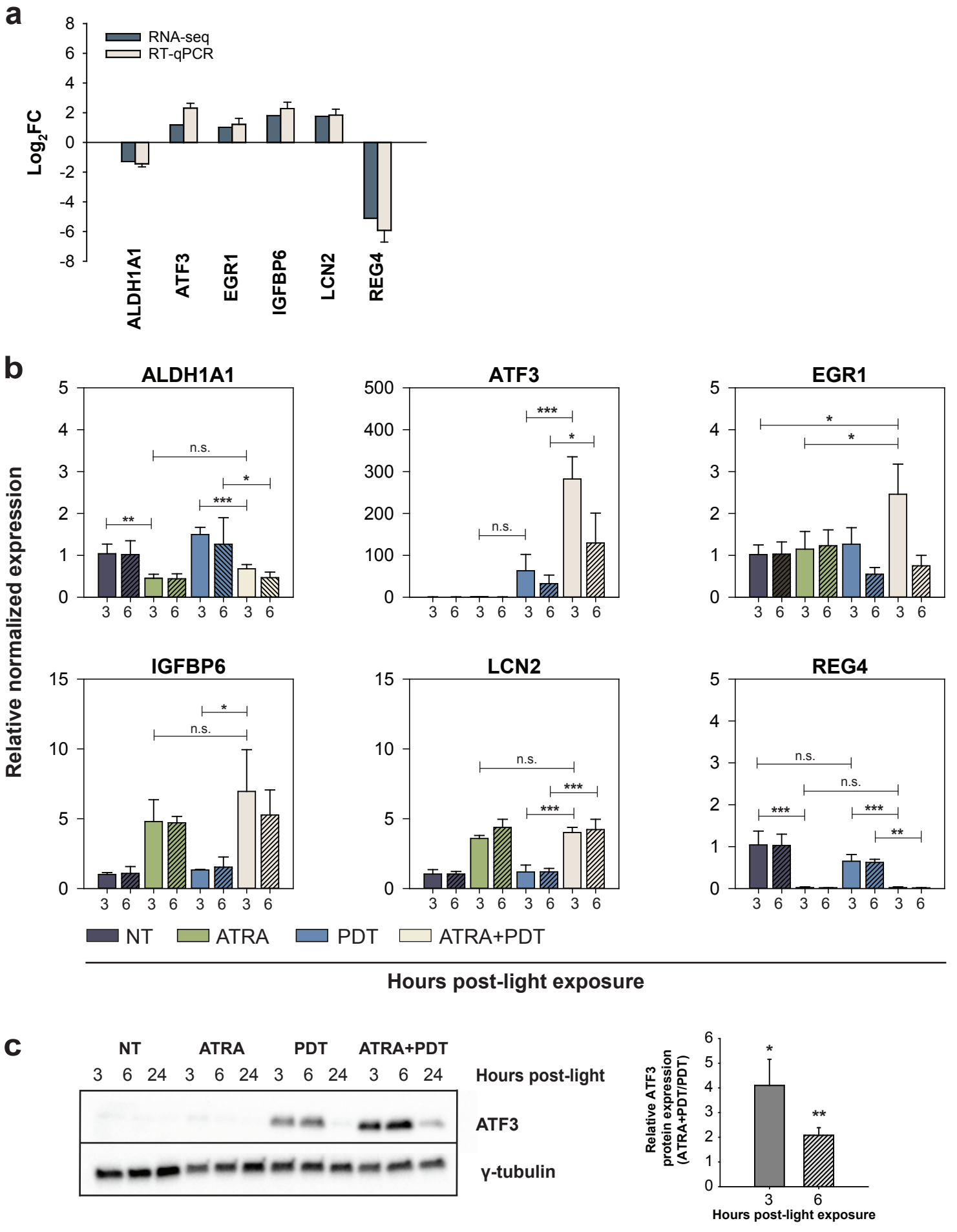
a
RNA-seq
RT-qPCR
Log2FC
ALDH1A1
ATF3
EGR1
IGFBP6
LCN2
REG4
b
Relative normalized expression
ALDH1A1
ATF3
EGR1
IGFBP6
LCN2
REG4
n.s.
NT
ATRA
PDT
ATRA+PDT
Hours post-light exposure
c
NT
ATRA
PDT
ATRA+PDT
Hours post-light
ATF3
γ-tubulin
Relative ATF3 protein expression (ATRA+PDT/PDT)
Hours post-light exposure

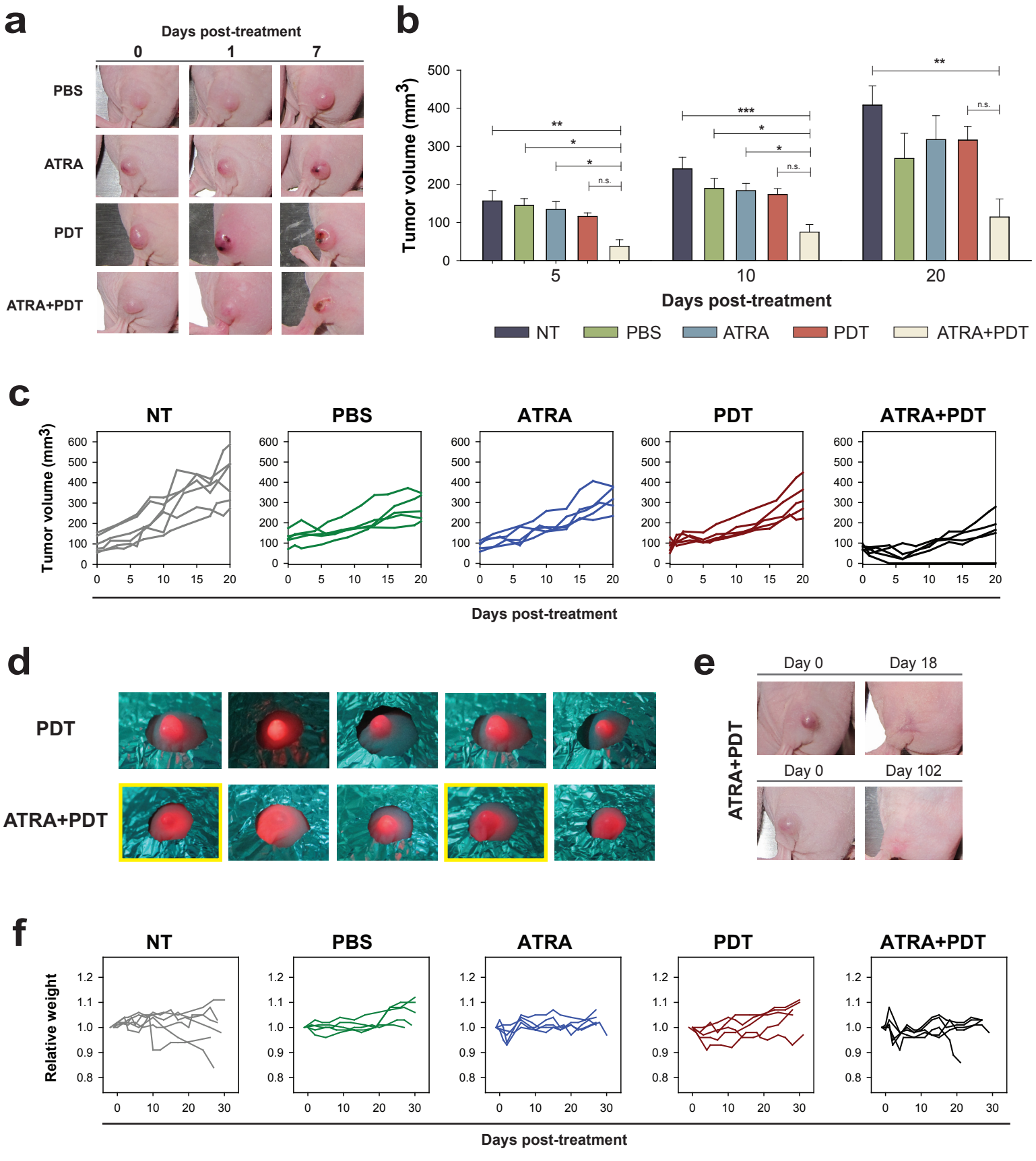
a
Days post-treatment
0
1
7
PBS
ATRA
PDT
ATRA+PDT
b
Tumor volume (mm3)
500
400
300
200
100
0
**
*
*
n.s.
***
*
*
n.s.
**
n.s.
5
10
20
Days post-treatment
NT
PBS
ATRA
PDT
ATRA+PDT
c
NT
PBS
ATRA
PDT
ATRA+PDT
Tumor volume (mm3)
600
500
400
300
200
100
0
0
5
10
15
20
Days post-treatment
d
PDT
ATRA+PDT
e
Day 0
Day 18
Day 0
Day 102
ATRA+PDT
f
NT
PBS
ATRA
PDT
ATRA+PDT
Relative weight
1.2
1.1
1.0
0.9
0.8
0
10
20
30
Days post-treatment